Carbon 129 (2018) 837–846

Contents lists available at ScienceDirect

Carbon

journal homepage: www.elsevier.com/locate/carbon

Chemistry below graphene: Decoupling epitaxial graphene from metals by potential-controlled electrochemical oxidation

Irene Palacio [a], Gonzalo Otero-Irurueta [a, c], Concepción Alonso [b], José I. Martínez [a], Elena López-Elvira [a], Isabel Muñoz-Ochando [d], Horacio J. Salavagione [d], María F. López [a], Mar García-Hernández [a], Javier Méndez [a], Gary J. Ellis [d], José A. Martín-Gago [a, *]

[a] Materials Science Factory, Dept. Surfaces, Coatings and Molecular Astrophysics, Institute of Material Science of Madrid (ICMM-CSIC), Sor Juana Inés de la Cruz 3, 28049 Madrid, Spain
[b] Dept. Applied Physical Chemistry, Autonomous University of Madrid, 28049 Madrid, Spain
[c] Centre for Mechanical Technology and Automation (TEMA), Dept. Mechanical Engineering, University of Aveiro, 3810-193 Aveiro, Portugal
[d] Institute of Polymer Science and Technology (ICTP-CSIC), Juan de la Cierva 3, 28006 Madrid, Spain

ARTICLE INFO

Article history:
Received 17 November 2017
Received in revised form
21 December 2017
Accepted 23 December 2017
Available online 27 December 2017

Keywords:
Graphene
Metals
Decoupling
Electrochemistry
Intercalation

ABSTRACT

While high-quality defect-free epitaxial graphene can be efficiently grown on metal substrates, strong interaction with the supporting metal quenches its outstanding properties. Thus, protocols to transfer graphene to insulating substrates are obligatory, and these often severely impair graphene properties by the introduction of structural or chemical defects. Here we describe a simple and easily scalable general methodology to structurally and electronically decouple epitaxial graphene from Pt(111) and Ir(111) metal surfaces. A multi-technique characterization combined with *ab-initio* calculations was employed to fully explain the different steps involved in the process. It was shown that, after a controlled electrochemical oxidation process, a single-atom thick metal-hydroxide layer intercalates below graphene, decoupling it from the metal substrate. This decoupling process occurs without disrupting the morphology and electronic properties of graphene. The results suggest that suitably optimized electrochemical treatments may provide effective alternatives to current transfer protocols for graphene and other 2D materials on diverse metal surfaces.

1. Introduction

The two-dimensional atomic structure of graphene is responsible for a wide assortment of superior properties combined in a single material [1,2]. In particular, its excellent charge-carrier mobility makes graphene a promising candidate for the construction of more efficient electronic devices. However, although the fabrication of a graphene-based fast transistor was announced in 2009 [3], this technology has not yet advanced to serial production status. One of the limiting factors for the step from basic research discoveries to real devices is the structural and chemical quality and reproducibility of the graphene sheet. From a technological perspective, Chemical Vapour Deposition (CVD) is undoubtedly the most convenient methodology to produce inexpensive, large area graphene sheets, but this process has the unavoidable requirement of a metallic surface, usually Cu or Ni, which quenches the electronic and optical properties of graphene, making the transfer to other substrates a necessary requirement to overcome this drawback. Several efficient transfer protocols have been developed [4,5], but even the best of these strategies induces significant structural and chemical defects (such as oxide groups) that impair the properties of graphene and subsequently limit the scope of its potential applications.

Over recent years there has been a major effort to develop new methodologies both to improve transfer efficiency or to avoid the transfer process altogether [6–9]. Among these methodologies, electrochemical detachment of the graphene layer has recently acquired some relevance [10–12]. For instance, there are voltammometric studies using the so-called “bubbling method” to decouple graphene from Pt and Ir [13,14] or the electrochemical detachment of graphene from Ru by hydrogen intercalation [15]. These protocols are essentially based on weakening the graphene-metal interaction by an electrochemically driven bubbling

* Corresponding author.
E-mail address: gago@icmm.csic.es (J.A. Martín-Gago).

https://doi.org/10.1016/j.carbon.2017.12.104

processes. These methodologies usually lead to efficient detachment of single layer graphene. However, they differ from the present case where the voltammetric electrochemical protocols are not employed to remove the graphene layer, but rather to induce oxidation of the supporting metal substrate, as a method to avoid subsequent physical transfer via PMMA, or other polymers. There have been many attempts to induce decoupling without removal of the layer in the past. Simple immersion in water for some hours in the case of Gr/Cu has been reported to lead to the formation of an oxide, leading to decoupled graphene flakes [8]. Also, insertion of atomic or molecular layers between the graphene and the supporting substrate from gases or adatoms has been reported to be an effective method for decoupling or modifying the properties of the graphene layer [16–18]. However, such intercalated atoms can be removed at relatively low temperatures in reversible processes that lead to unstable interfaces, with possible etching processes occurring at higher temperatures [17,18]. To improve these aspects, other protocols have explored the idea of direct oxidization of the interface between the metal support and the graphene layer. Lizzit et al. and others have employed thermal treatments under an oxygen atmosphere to decouple graphene from metals [19–22].

Currently, the most effective methodology for growing perfectly ordered and pure graphene takes advantage of the catalytic properties of a metal, in well-controlled ultra-high vacuum (UHV) environments, to thermally decompose either hydrocarbons or organic molecules [23,24]. As well as several advantages (scalability, powerful *in situ* characterization, highly epitaxial and impurity-free), the strong coupling between the metal substrate and the graphene layer is a recurring drawback [25]. The work presented shows that by an inexpensive and easily scalable electrochemical process, highly perfect graphene samples epitaxially grown in UHV on metal surfaces can be decoupled by controlled oxidation that takes place exclusively on the metal surface with minimal disruption of the graphene morphology or structure. By a combination of experimental techniques and theoretical methods, the decoupling of high-quality epitaxial graphene on the tens-of-micrometer scale from a Pt(111) substrate by the gentle intercalation of sub-monolayer hydroxide on the Pt surface is demonstrated. This methodology could represent a significant step towards the use of readily grown graphene on both single-crystal and polycrystalline noble metal surfaces for practical applications avoiding transfer processes. To illustrate the universality of the process, graphene was also successfully decoupled from Ir(111).

2. Methods

2.1. UHV graphene preparation and in situ characterization

An UHV system with a base pressure of 1×10^{-10} mbar, equipped with an Omicron room temperature Scanning Tunnel Microscope (STM) and an Omicron Low Energy Electron Diffraction (LEED). Pt(111) and Ir(111) surfaces were cleaned by repeated cycles of argon ion sputtering and annealing in an oxygen atmosphere (T = 1200 K for Pt(111) and 1373 K for Ir(111) and $P_{oxygen} = 5 \times 10^{-8}$ mbar). In order to avoid any residual oxygen on the surface, several extra cleaning cycles were carried out without oxygen. The pressure during the last annealing cycle was lower than 7×10^{-10} mbar. STM and LEED were used to assess the cleanliness of the surfaces. The graphene layer was grown by decomposition of fullerenes (Sigma-Aldrich, 99% of purity) at high temperature (1150 K) following our calibrated protocols to ensure saturation coverage [24,26]. Some samples were grown by thermal decomposition of ethylene with similar results. WSxM software was used for data acquisition and analysis [27].

2.2. Electrochemical treatment

An electrochemical cell with a 3-electrode setup was used [28]. A platinum wire (99.99% purity) served as the auxiliary electrode. All potentials are quoted with respect to the Ag/AgCl reference electrode. The area of the working electrode (Pt(111) or Ir(111)) that was exposed to the solution was 0.33 cm^2 in all experiments. Cyclic voltammetry experiments were performed with an Autolab PGSTAT 30 potentiostat from Eco-Chemie. The electrolyte employed was 0.1 M $HClO_4$ and the scan rate was 0.05 V s^{-1}.

2.3. Atomic force microscopy (AFM)

AFM measurements were performed *ex situ* at room temperature and ambient conditions employing a Nanotec AFM with a PLL/dynamic measurement board. AFM images were recorded in dynamic amplitude modulation (AM) and contact modes. WSxM software was used for images and curves acquisition and processing [27]. Aluminium coated silicon cantilevers (Budget Sensor k = 3 N/m, $\nu_0 = 70$ kHz) were used.

2.4. Scanning electron microscopy (SEM)

The SEM micrographs were recorded on a FEI Nova NanoSEM 230 microscope. The micrographs were measured at 25.000x magnification and using a VCD detector, which is a backscatter electrons detector for high contrast images at low potentials.

2.5. Raman

Raman measurements were undertaken *ex situ* in the Raman Microspectroscopy Laboratory of the Characterization Service in the Institute of Polymer Science & Technology (CSIC) using a Renishaw InVia Reflex Raman system (Renishaw plc., Wotton-under-Edge, U.K.) comprising a grating spectrometer with a Peltier-cooled charge-coupled device (CCD) detector, coupled to a confocal microscope. All spectra were processed using Renishaw WiRE 3.4 software. The Raman scattering was excited using an argon ion laser wavelength of 514.5 nm. The laser beam (laser power at the sample ≈ 1 mW) was focused onto the sample with a 50x (N.A. = 0.75) microscope objective, and multiple scans were accumulated at an exposure time of 10s.

2.6. X-ray photoemission spectroscopy (XPS)

XPS measurements have been carried on in two different systems, in both of them using a hemispherical analyzer SPECS Phoibos 100 MCD-5 in UHV systems at a base pressure in the range of 10^{-10} mbar. A twin anode (Mg and Al) X-ray source was operated at a constant power of 300 W using Mg K_α radiation ($h\nu = 1253.6$ eV) and monochromatic Al K_α radiation ($h\nu = 1486.6$ eV).

2.7. Computational modelling

Density Functional Theory (DFT)-based calculations were performed by using the efficient plane-wave code QUANTUM ESPRESSO [29]. The calculations account for an empirical efficient van der Waals (vdW) R−6 correction (DFT + D approach [30,31] to add dispersive forces to conventional density functionals. For this purpose, we have used the revised version of the generalized gradient corrected approximation of Perdew, Burke, and Ernzerhof (rPBE) to account for the exchange-correlation effects (XC) [32]. Within this atomistic simulation package the Kohn-Sham equations are solved using a periodic-supercell geometry. Rabe-Rappe-Kaxiras-Joannopoulos (RRKJ) ultrasoft pseudopotentials [33,34]

have been used to model the ion-electron interaction in the H, C, O and Pt atoms. For all the systems analyzed in the present work the Brillouin zones (BZs) have been sampled by means of: i) [8 × 8 × 1] monkhorst-Pack grids [35] for the structural and lattice optimizations, and ii) [64 × 64 × 1] monkhorst-Pack grids for the electronic structure calculations (such a highly-dense k-point grid discretization turns into necessary to electronically reproduce the graphene Dirac-cone). The one-electron wave-functions are expanded in a basis of plane-waves with energy cut-offs of 400 and 500 eV for the kinetic energy and for the electronic density, respectively, which have been adjusted to achieve sufficient accuracy to guarantee a full convergence in total energy and density

Both structure and lattice have been simultaneously fully-optimized for all the systems involved in the present study (see the supplementary information for further details): clean Pt(111) and $Pt_n(OH)_m$@Pt(111) surfaces, and Gr/Pt(111) and Gr/$Pt_n(OH)_m$@Pt(111) interfaces (with ratios m/n = 1/8, 1/4, 1/2, 5/8, 3/4 and 1 ML of homogeneous intercalated-OH content. Note that in this notation m/n = 1/2 equals 1 ML of Pt_2OH).

Structural and lattice optimizations, as well as electronic structure calculations, have been performed for rectangular (6 × 2) and (4 × 2) Pt(111) unit cells for Gr/Pt(111) and Gr/$Pt_n(OH)_m$@Pt(111) interfaces, respectively, to mimic the extended Pt(111) surface and an infinite covering SLG sheet with a 0° rotation between Pt substrate and Gr. The choice of this rectangular lattice to perform the calculations has been made to get access, from the configurational point of view, to the most homogeneous intercalated-OH coverages possible according to previous literature [36]. In order to verify the reliability of the results obtained with this rectangular lattice we have examined a $(\sqrt{3} \times \sqrt{3})R30°$ graphene commensurate with the Pt(111) substrate similar to that previously reported by our group [24] obtaining equivalent results, which justifies the validity of our choice.

3. Results and discussion

Epitaxial graphene was grown on Pt(111) following the procedure described elsewhere [24,26,37]. STM images clearly show that a single-layer high quality graphene (Gr) sheet covers the whole Pt(111) surface. Fig. 1a shows a representative STM image of a wide scanned area as well as the standard LEED pattern taken at 75 eV (inset) obtained for Gr on Pt(111) [23,26]. In the image, various morphological features such as a wrinkle, nanobubbles and grain boundaries can be observed, as have been previously reported for these materials [38,39]. More details on these features are provided in the supplementary information. Moreover, high-resolution STM images, like that presented in Fig. 1b and acquired on atomically flat terraces, show atomic resolution at the Gr layer and the presence of a moiré superstructure, a clear indication of single layer Gr growth [26]. Thus, both STM and LEED results clearly indicate the high quality of the graphene layer produced, and employed in the subsequent experiments.

After *in situ* characterization, the samples were removed from the UHV preparation chamber and characterized *ex situ* using Raman spectroscopy, XPS, AFM and SEM. Subsequently, electrochemical oxidation was applied followed by full characterization of the modified systems employing the same aforementioned techniques in order to confirm the integrity of the graphene layer and to study the nature of the decoupling process.

Electrochemical oxidation is much less invasive than thermal oxidation and has been widely studied for different metallic surfaces by cyclic voltammetry [40]. In fact, the voltammetric profile for metals, such as single-crystal platinum surfaces in non-adsorbing electrolytes, is well established and presents a characteristic shape [41]. All studies point out that the Pt(111) electrode is electrochemically oxidized in a complex process involving several pH dependencies and oxidation steps, between 0.6 V/reversible hydrogen electrode (RHE) and the onset of O_2 evolution at about 1.5 V [42]. However, there are some discrepancies about the origin and nature of the species involved in the complex voltammetric shape [43,44]. The aim of the present work was to expose the metal surface, covered by a homogeneous graphene layer, to a voltammetric oxidation cycle that oxidizes the metal interface below the graphene layer.

Fig. 2a shows the voltammograms of the clean Pt(111) surface and the graphene covered Pt (111) surface after applying an electrochemical protocol in 0.1 M aqueous $HClO_4$ that consists of an anodic potential scan from 0.36 to 1.05 V followed by a cathodic potential scan from 1.05 to 0.7 V (0.6 V for clean Pt(111)). A scan rate of 0.05 V s^{-1} was selected to control the oxidation reaction kinetics and the anodic potential was varied to obtain the optimal conditions for decoupling graphene from Pt, avoiding side reactions such as the evolution of CO_2 and O_2, or the creation of defects in the graphene network. The shape of the voltammograms clearly indicates that an oxidation reaction has taken place, and the charge required for oxide formation can be obtained by integrating the oxidation peak. For the clean Pt(111) surface (grey curve in Fig. 2a) the oxidation charge is 101.5 μC cm^{-2}, which corresponds to the formation of about 1 ML Pt_2OH (as it will be shown below). The presence of the monolayer of graphene delays the oxidation

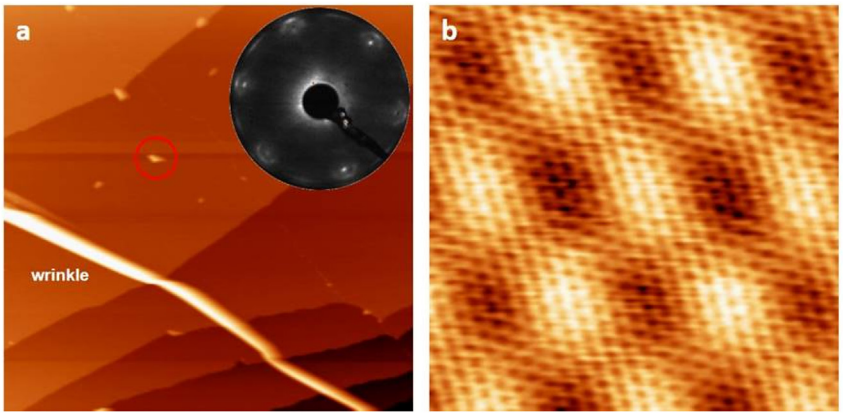

Fig. 1. a) STM image of a wide scanned area ((200 × 200) nm^2, I = 0.15 nA, V = 750 mV). The graphene layer covers the whole surface. In the image, a wrinkle and several nanobubbles (such as that circled in red) can be observed. The inset shows the typical LEED pattern of Gr on Pt(111) taken at 75 eV b) High resolution STM image acquired from a flat terrace ((4 × 4) nm^2, I = 4 nA, V = 10 mV) showing a characteristic moiré superstructure with atomic resolution. (A colour version of this figure can be viewed online.)

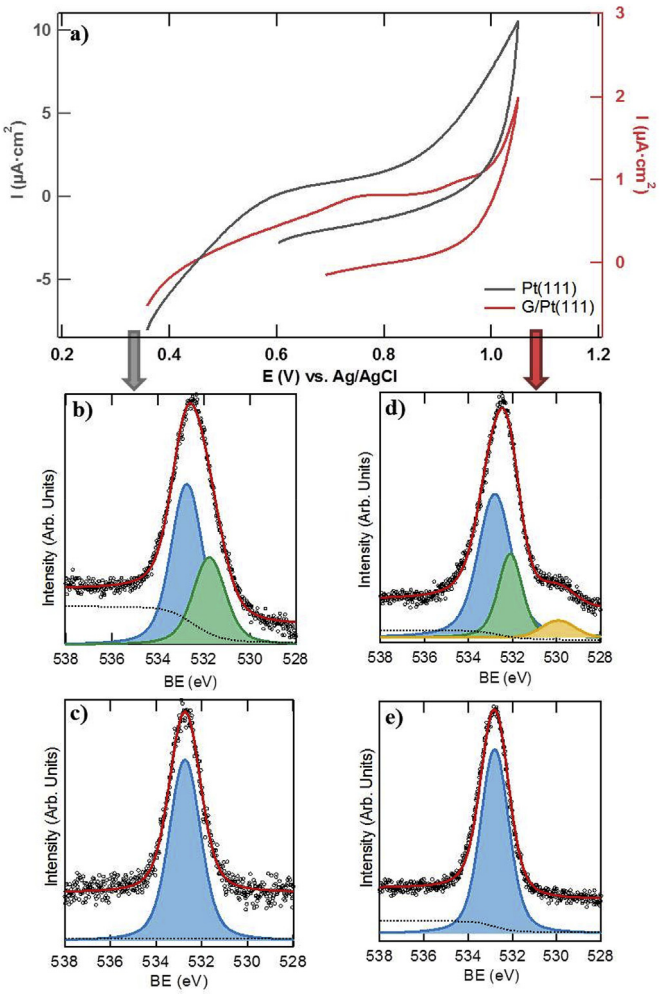

Fig. 2. a) Cyclic voltammetry of a Pt(111) and a Gr/Pt(111) samples in 0.1 M aqueous $HClO_4$. A Pt_2OH sub-monolayer is formed beneath the graphene sheet (scan rate 0.05 V s^{-1}). b) and d) O1s XPS spectra after the aforementioned electrochemical treatment of b) clean Pt(111) sample and d) Gr/Pt(111) sample. Two main components can be seen: the blue areas correspond to oxides and the green areas to adsorbed species. c) and e) O1s XPS spectra after annealing the previous samples at 973 K. The adsorbed species (green) disappear and only oxide species remain. (A colour version of this figure can be viewed online.)

process and makes it necessary to apply higher over-potentials. Thus, the charge required for the oxide formation, obtained by integrating the oxidation peak, is 32 μC cm^{-2} for our protocol, considerably lower than that of the clean surface. However, although the coverage is low, about 0.25 ML, this is sufficient to decouple the graphene layer, as will be demonstrated below. Whilst graphene can act as a barrier, the water molecules are able to diffuse to the metallic substrate via surface defects, as was reported by Feng et al. [45]. Moreover, recent reports claim that chemistry below graphene, such as CO oxidation on Pt(111), can take place very efficiently on a metallic surface covered by a single-layer graphene due to a confinement effect [46,47].

The O1s XPS spectra of Pt(111) and Gr/Pt(111) samples confirm the oxidation of the platinum surface after the electrochemical treatment. Fig. 2 shows the O1s core-level peaks of a clean (Fig. 2b) and graphene covered Pt(111) surface (Fig. 2d) after the treatments represented by the voltammograms of Fig. 2a. The best fits are also included. In both cases, the less intense green component (at 531.7 eV for the Pt sample and at 532.1 eV for the Gr/Pt sample) can be ascribed to hydroxide species adsorbed on the surface [48] and the blue curve (at 532.7 eV for Pt and 532.8 eV for Gr/Pt) to the OH covalently bonded to the Pt surface. Surprisingly, the ratio between each component is similar for both samples. The assignment of the binding energies (BE) to the chemical species is clear. The more intense blue component appears with a binding energy that is intermediate to those reported for OH and water, both adsorbed on the platinum surface [49,50]. Spectra recorded after subsequent annealing of these two surfaces up to 973 K reveal that this is the only remaining component, thus it cannot be assigned to any adsorbed species but rather to one covalently bonded to the surface (see Fig. 2c,e). Moreover, the possible formation of a pure PtO or PtO_2 can be dismissed since the reported binding energies for the O1s are significantly lower, around 530 eV [51]. In the case of the Gr/Pt sample a new component appears at 529.9 eV (yellow peak), which can be ascribed to residual C=O species [48] that disappear upon annealing (Fig. 2e). The Pt4f core level lineshape is discussed in the supplementary information.

Contrary to previous assumptions in the literature of metal-oxide formation (PtO or PtO_2), the XPS results here show that the voltammetric profile is related to the reversible formation of hydroxide from the electrochemical dissociation of water [49]. The chemical reaction at the electrode surface would be then:

$$H_2O + (*) \leftrightarrow OH_{ads}(*) + H^+ + 1e^- \quad (1)$$

where (*) represents a free Pt(111) adsorption site.

In a second step the OH_{ads} reacts with the free platinum adsorption sites to form the hydroxide species. With the experimental conditions used in the electrochemical process, our results support the formation of an incomplete Pt_2OH layer underneath graphene.

Prior and subsequent to the aforementioned electrochemical treatment, the samples were characterized *ex situ* using Raman microspectroscopy, XPS and AFM. Fig. 3a shows representative *ex situ* Raman spectra of graphene on Pt recorded before and after electrochemical decoupling of graphene from the Pt surface. The Raman data obtained are, in a first instance, puzzling and do not adjust to general interpretations found in the scientific literature. Before the decoupling process, no evidence of the G and 2D bands characteristic of free-standing graphene was observed (see Fig. 3a, black curve), and only two sharp bands at 1556 and 2331 cm^{-1} could be seen, corresponding to atmospheric O_2 and N_2, respectively [52]. Several previous Raman studies of Gr on Pt substrates have appeared in the literature. Kang et al. [53] reported that the graphene D, G and 2D bands could only be observed very weakly, at 1355, 1605 and 2720 cm^{-1}, respectively, and this behaviour was ascribed to an unexplained strong Pt-metal interaction related with an electronic hybridization between the graphene Dirac cone states and platinum d-orbitals [54]. However, it should be noted that the Pt-G interaction is considered to be "weak" because the π-bands at the Dirac points are conserved, slightly shifted with respect to pristine graphene, and the XPS core-level shifts are small [23,55] with respect to other transition metals. Whilst, as in our case, the complete absence of spectral features from graphene is surprising, this phenomenon has been previously reported [54,56,57]. Indeed, a detailed study of the effect of metal substrates on the Raman spectra of CVD graphene showed that the Raman features of Gr on Pt are strongly suppressed when compared to other metallic substrates such as Cu, Au and Ag. Evidence suggested that quenching of the Raman bands on metal surfaces can be associated, in most cases, to electromagnetic screening from reduced optical fields arising from substrate electromagnetic anti-resonance [57]. On the other hand, it has also been described that the intensity of the Raman signal on Pt can be intimately associated with the growth method, as demonstrated recently by Yao et al. [58] who observed a

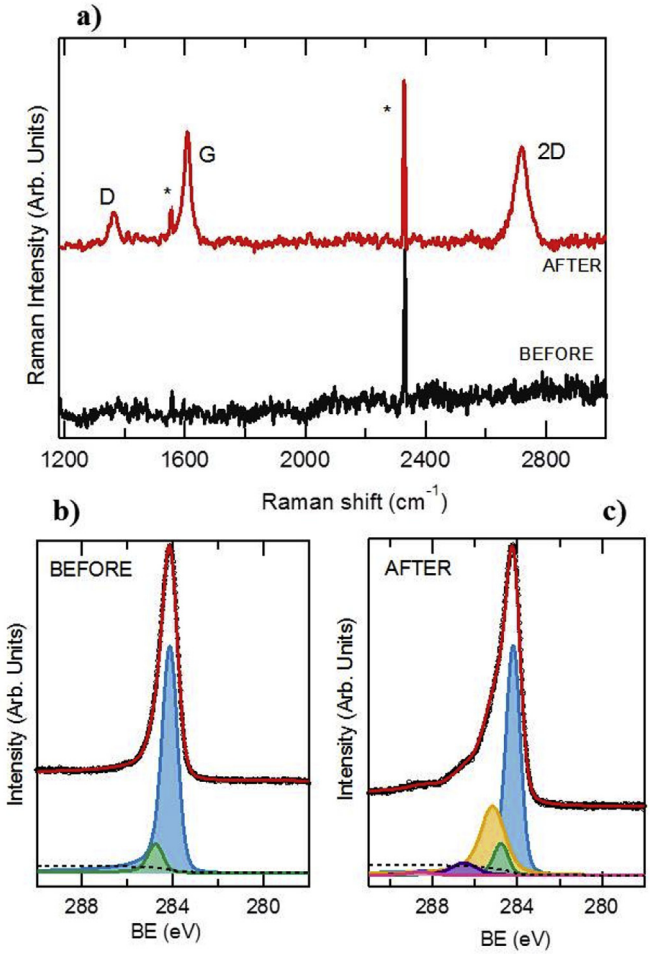

Fig. 3. a) Raman spectra of graphene on Pt(111) before (black curve) and after (red curve) electrochemical oxidation. The decoupling of the graphene sheet from the metallic substrate is clear by the emergence of D, G and 2D bands. b), c) C1s XPS spectra of the Gr/Pt(111) sample before (b) and after (c) the electrochemical oxidation. (A colour version of this figure can be viewed online.)

near-ideal band structure of Gr grown with a very low carbon concentration under very high annealing conditions.

Radical changes were observed in the *ex situ* Raman spectra obtained from the electrochemically treated samples (see Fig. 3, red upper trace) where the characteristic features of graphene are now clearly observed; the G-band, corresponding to a doubly degenerate (iTO and LO) phonon mode (E_{2g} symmetry) at the Brillouin zone centre, appears at around 1605 cm^{-1}; the disorder-induced D band, due to the six-atom ring breathing modes arising from a iTO phonon activated by a defect, involving an intervalley double-resonance process, is found at 1360 cm^{-1}; and the second order 2D band appears at around 2720 cm^{-1} [59–62]. It should be pointed out that the D, G and 2D band positions are somewhat shifted when compared to the typical values observed with a 2.41 eV (514.5 nm) laser source for free-standing single-layer graphene (SLG), of 1350, 1580 and 2700 cm^{-1}, respectively. Upshifted G modes have been associated with both doping and mechanical stress [59]. When multiple spectra recorded from different regions of an electrochemically treated Gr/Pt surface are compared (see supplementary information, figure S1.1), the G-peak values vary in general between 1605 and 1615 cm^{-1}, suggesting zones with high strain, to values as low as 1587 cm^{-1}, much closer to the values reported for unperturbed, free-standing graphene. However, the bandwidth (FWHM) is quite broad ranging from 22 to 35 cm^{-1}. The D and 2D peak values also appear at various frequencies, ranging from 1350 to 1380 cm^{-1} in the former, when observed, and between 2720 and 2735 cm^{-1} in the latter.

While the intensity of the D-band is generally low in most spectra, and the FWHM varies from 35 to 50 cm^{-1}, it should be pointed out that due to our particular growth mode, many different rotational domains can appear [26] that can lead to an increase in the D band intensity, which are not, in principal, associated to a more defective graphene surface. On the other hand, the 2D band is quite symmetrical in all cases consistent with a monomodal spectral response corresponding to SLG, and the FWHM varies between 50 and 70 cm^{-1}. Such large line broadening is always observed in all cases when graphene is grown in UHV on Pt, Ir and other transition metals [54,63] and is most likely to be associated with increased stresses. This unusual behaviour in the Raman spectra has been reported previously for epitaxial graphene grown in UHV conditions [57], and it has been suggested that the interaction C-Pt may be strong at discreet atomic positions of the moiré superstructures, where covalent bonding may induce a rupture of the sp^2 hybridization into sp^3. These points are also known to be interacting channels that may be responsible for the increase in the Raman D peak and the broadening of the FWHM and blueshifts in the G and 2D Raman peaks [26,37,64] on decoupling the graphene sheet from the metal surface.

Fig. 3b,c shows the XPS results of the C1s core-level peak of graphene before and after electrochemical oxidation. The fit of the sp^2 C1s peak was performed using a Doniach-Šunjić line shape using an asymmetry parameter of 0.068 [65]. The remaining components were fitted using Gaussian-Lorentzian lines. Before treatment (Fig. 3b) the C1s peak has one main component associated to sp^2-graphene at 284.1 eV. The small feature at 284.7 eV is assigned to sp^3 bonds [66,67], that in our case arise principally from the grain boundaries of the different rotational graphene domains typical of this type of graphene synthesis [26,68]. In the C1s peak after treatment (Fig. 3c) the main sp^2 component remains unaltered, confirming that no sample damage was induced. A shift towards lower binding energies of the sp^2 component has been previously reported for oxygen intercalated below graphene [22,69]. This shift has been related to the interaction of the graphene layer with the oxygen atoms beneath. Since in our case the graphene interacts with hydroxyl molecules instead of oxygen atoms the expected shift will be very low (of the order of the experimental resolution). Three new components appear weakly at 285.1, 286.5 and 288.5 eV and are assigned to C-OH, C-O and C=O respectively [37,48,67] arising from contamination. Since the sample was removed from UHV to undertake both the *ex situ* characterization and the electrochemical treatment, these contaminant signals are clearly expected in a highly surface sensitive technique such as XPS, and the contamination could be easily removed by gentle annealing, or even by scanning with an AFM tip (see supplementary information; figure S2.1).

The AFM images, acquired in air before and after electrochemical oxidation, indicate that the main morphological features of the Gr layer are preserved (Fig. 4a and d). Figure 4a shows the surface of the Gr/Pt sample before treatment, and apart from the typical surface monoatomic steps, the main features consist of large graphene wrinkles and some bumps randomly scattered along the surface. The presence of these long wrinkles are the evidence for the presence of graphene, as they are one of its main distinctive characteristic features in SPM analysis, and are formed due to distinct thermal expansion of the graphene and the substrate material. The presence of these wrinkles is also confirmed by SEM images that show graphene patches of the order of microns (see supplementary information; figure S3.1). Except for a slight

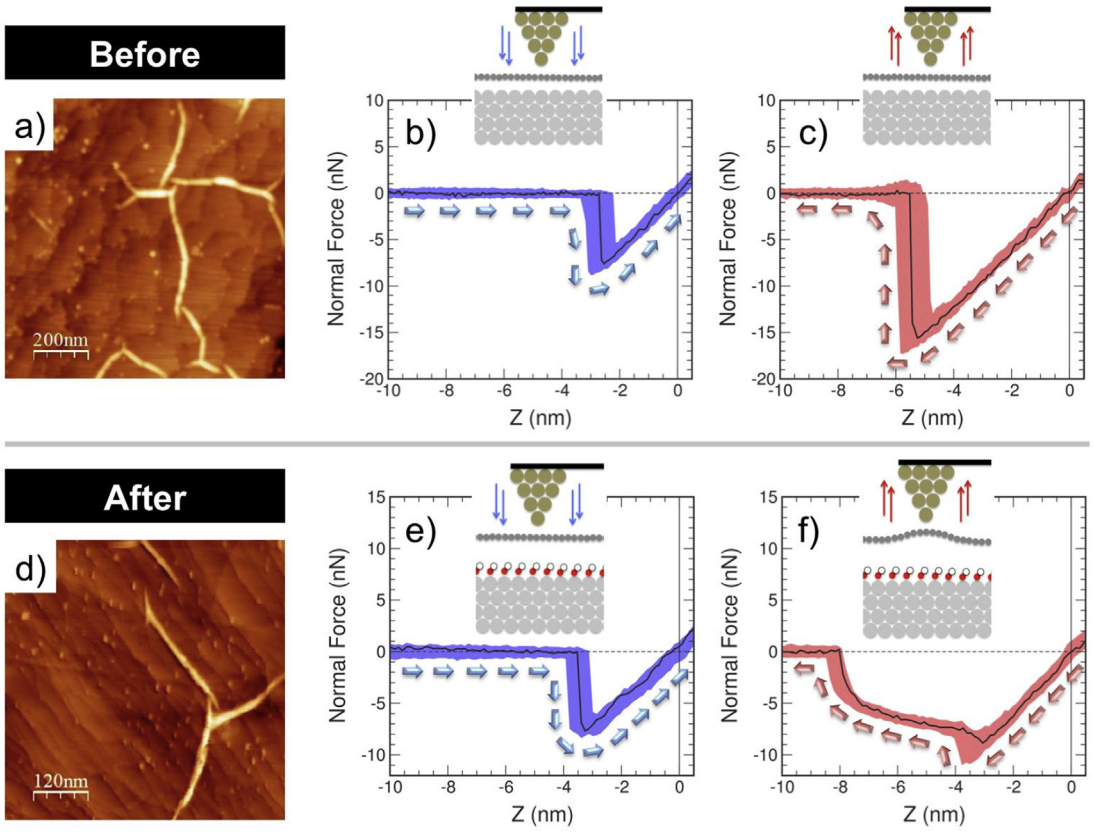

Fig. 4. AFM characterization of a Gr/Pt(111) sample before and after the electrochemical treatment. Black lines correspond to a typical curve while the coloured areas represent >100 repeated curves. Arrows indicate the direction of the recorded plot. a) AFM image (1×1) μm^2 measured ex situ in dynamic (AM) mode before the electrochemical treatment. Graphene wrinkles and platinum steps are visible. b) Force-distance plot in forward direction (approaching) showing the characteristic jump-to-contact from zero-force and the sloped straight-line of contact. c) Corresponding retracting curve (withdraw) where a higher force is achieved due to the adhesion force. d) AFM image (600×600) nm^2 measured after the electrochemical treatment in contact mode. Graphene wrinkles and steps are present. e) Force-distance plot in forward direction showing a similar jump-to-contact. f) Force-distance plot in retracting direction showing a different behaviour: the adhesion force is reduced and a bump in the force is perceived. (A colour version of this figure can be viewed online.)

roughening of the steps, the main morphological features of the graphene grown in UHV are preserved after sample exposure to ambient conditions (compare STM images in Fig. 1a and AFM image in Fig. 4a). The sample after electrochemical treatment is shown in Fig. 4d. Wrinkles of similar length are still visible; thus, the electrochemical oxidation process does not appear to disrupt the Gr morphology.

The major changes upon electrochemical oxidation can be appreciated in the F(z) curves (Fig. 4b–c,e-f) where a typical curve (in black) and coloured area corresponding to > 100 experiments are represented. Before treatment (Fig. 4b and c) the F(z) plot corresponds to a typical force curve [70] between a tip and a rigid substrate recorded in air where, when approaching, the forward curve (Fig. 4b) manifests a jump to contact, followed by the characteristic linear increase of the force with tip-sample displacement. The backward curve (Fig. 4c) also shows the characteristic hysteresis due to adhesion forces [70].

However, F(z) curves recorded after electrochemical treatment (Fig. 4e and f) show distinctive features. While the forward curves (Fig. 4e) are very similar to those acquired before the electrochemical oxidation, when withdrawing the tip the shape of the F(z) curves changes dramatically. At the curve minimum a small v-shaped feature is observed that can be assigned to the initiation of the detachment from the rigid surface, which is followed by a long rounded-shaped feature that implies a smooth variation of the force with the displacement consistent with the presence of a soft membrane between the tip and the substrate. This must correspond to the displacement of the whole graphene layer that remains adhered to the AFM tip during retraction. Although it is observed that this process extends for 3 nm or more, the attraction between the tip and the graphene sheet produces a local deformation that separates the graphene layer from the substrate, thus the distance value between the decoupled graphene layer and the platinum surface appears to be larger than it actually is. Therefore, clearly the spectroscopic F(z) analysis provides strong evidence to support that the electrochemical treatment employed structurally decouples the graphene from the Pt(111) substrate. The analysis of the AFM images as well as the mapping of the F(z) curves, the charge transferred in the voltammogram and the Raman spectra (see supplementary information) performed over the whole surface, indicate graphene decoupling over most of the sample, approximately 80–90%, remaining anchored to the substrate only in some small areas, mainly near to the wrinkles (aprox. 20-10%). In the areas adjacent to the wrinkles, due to their folded structure, the graphene is more intimately “attached” to the surface making it difficult for water to intercalate and thus even more difficult for decoupling to take place. Wrinkles are formed by differential thermal expansion during the cooling down process, as the metal contracts more than the graphene layer. They are one of the main drawbacks in the technological applicability of graphene and, unfortunately, are inherent to the formation of the graphene layer [71,72]. Therefore, these small coupled areas are inevitable.

However, it should be stressed that at an atomic level there may also remain some local pinning points in the middle of the terraces, as electrochemistry indicated that oxygen coverage is as low as 0.25 ML, yielding a subtle interfacial chemical interaction [64].

To demonstrate that the decoupling of graphene by potential-controlled electrochemical oxidation is effective in other metals, we have repeated the experiments for a Gr/Ir(111) sample. Graphene was grown the same way. Fig. 5a shows an STM image of the Ir (111) sample completely covered by 1 ML of graphene exhibiting a typical moiré superstructure. In the inset a zoom in one of the terraces points out the high quality of the graphene layer. The electrochemical oxidation protocol applied to the samples was equivalent to the one of Pt(111), however in some aspects it is different since the substrate, and therefore the oxidation conditions, changed. We used a scan rate of 0.05 V s^{-1} and an anodic potential scan from 0.2 to 1 V followed by a cathodic potential scan from 1 to 0.9 V [73]. The oxidation charge obtained is 140.8 μC cm^{-2} [74] which approximately corresponds to 0.4 ML of $Ir(OH)_3$. Due to the different hydroxide species formed in Pt(111) and in Ir(111) a straightforward comparison of the charges cannot be done. After the electrochemical treatment, the O1s XPS spectrum (Fig. 5b) proves that the oxidation on the iridium surface was effective, presenting the same components already described for the case of the Gr/Pt(111) samples (Fig. 2b). The blue component at 532.7eV was assigned to the OH covalently bonded to the Iridium surface, the green one at 532 eV to the adsorbed hydroxide species and the yellow one at 530 eV to the residual C=O species [48]. C1s core level (not shown) preserves its sp^2 component proving the graphene sample is not damaged during the treatment. Moreover, the samples were also characterized with AFM and Raman (not shown) before and after the treatment to check the stability of the graphene layer towards the electrochemical oxidation. The behavior was found to be similar to that observed with the platinum sample.

Finally the F(z) curves taken with the AFM before and after the treatment (Fig. 5c) show again the same behavior as that already discussed for the Gr/Pt(111) samples. In this case the horizontal part of the plot (backward direction, red plot Fig. 5 c) is significantly larger, showing that the area of the decoupled graphene layer is larger and therefore the pulling distance is longer.

In order to shed some light on the structural and electronic decoupling process of graphene from the Pt(111) substrate as the intercalated-OH content increases in between the Gr/Pt interface, we have carried out a large battery of Density Functional Theory (DFT)-based calculations (see *Methods*).

After full structural and lattice relaxations this formalism yields lattice parameters for bulk fcc of platinum surface of 2.79 Å and for a free-standing graphene of 2.46 Å. Interestingly, the lattice optimization for the Gr/Pt(111) and Gr/$Pt_n(OH)_m$@Pt(111) interfaces (once formed) reveals an average 2D *XY* contraction of the Pt layers of around a 4% (from 2.79 to 2.68 Å) and a slight vertical *Z* expansion of around a 3% (from 2.79 to 2.87 Å), which permits to accommodate a perfectly commensurate SLG (single layer graphene) sheet with a maximum expansive strain of around 4% (from 2.46 to 2.55 Å), in good agreement with previous literature [75]. It is important to remark that an important amount of 12 and 9 Pt physical layers were necessary to obtain perfectly converged results in geometric and electronic structure for the Gr/Pt(111) and Gr/$Pt_n(OH)_m$@Pt(111) interfaces (see Fig. 6a–b), respectively. Under these conditions for the Gr/Pt(111) interface the graphene layer remains at a relatively large distance from the outermost Pt(111) layer of 3.31 Å, and retains a quite atomically flat surface with buckling < 0.05 Å, in agreement with reference [55].

Regarding the $Pt_n(OH)_m$@Pt(111) surfaces, the result of the relaxations reveals that in all cases the intercalated OH groups strongly bind to the Pt(111) surface, and are located at “on-top” Pt sites at an average distance from the Pt surface of 2.15 Å, yielding perfectly stable configurations where visible OH-OH dipolar interactions emerge to orientate the OH groups and maximize the surface energy (see Fig. 6b). Computed adsorption energies of the OH groups on the different $Pt_n(OH)_m$@Pt(111) surfaces for the previously mentioned (m/n) ratios range between 2.42 and 2.58 eV, are in excellent agreement with previous literature on similar configurations [36]. Moreover, Ferrighi et al. have very recently reported a viable DFT-based H_2O on-surface dissociation mechanism on Cu(111) and Pt(111) in defective-Gr/(Cu/Pt) interfaces, where one of the stable dissociation products are chemisorbed OH groups on the metal surfaces [76].

Fig. 6c shows the average Gr—Pt(111) surface perpendicular distance (in Å) as a function of the intercalated-OH coverage (in ML units). In the figure a significantly large jump can be seen in the Gr—Pt(111) distance from 3.31 to 4.98 Å between 0 ML and 0.125 ML, associated to the presence of the starting amount of OH groups chemisorbed on the Pt(111) surface that, from the experimental perspective, may be seen as the first formation stages of intercalated-OH chemisorbed groups. It is important to note that 0.125 ML of OH corresponds to the experimentally determined value of 0.25 ML of Pt_2OH. Also, in Fig. 6c a continuously increasing trend in the Gr—Pt(111) surface perpendicular distance can be

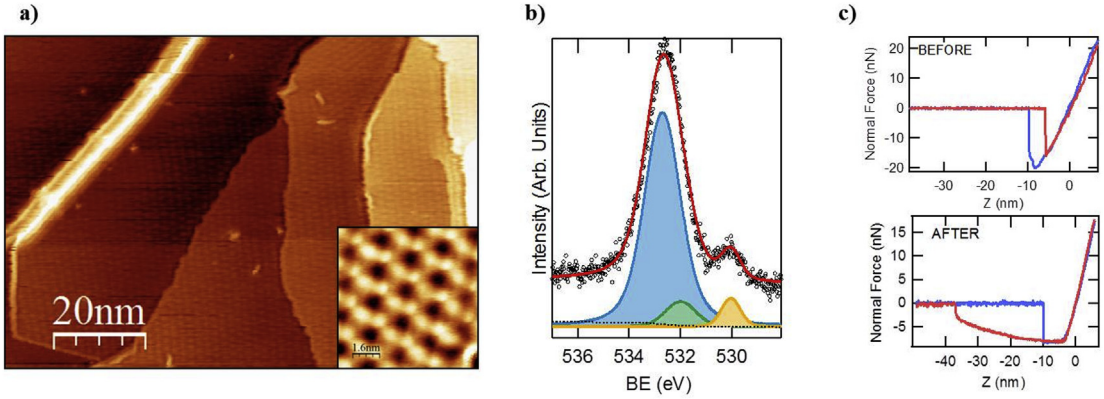

Fig. 5. a) Large STM image of Gr/Ir (111). (100 × 70) nm, 2 V, 62 pA. The whole Ir (111) is covered by 1 ML of graphene. The typical moiré is visible and also on the top left corner of the image a wrinkle. In the inset a zoom in one of the terraces, (8 × 8) nm, 0,03 V b) O1s XPS peak of the Gr/Ir(111) sample after the electrochemical treatment fitted with 3 main components (blue areas correspond to the hydroxides, green and yellow to the adsorbed species. c) F(z) curves of the samples (blue forward and red backward direction) before and after the treatment showing changes related with the decoupling of graphene. (A colour version of this figure can be viewed online.)

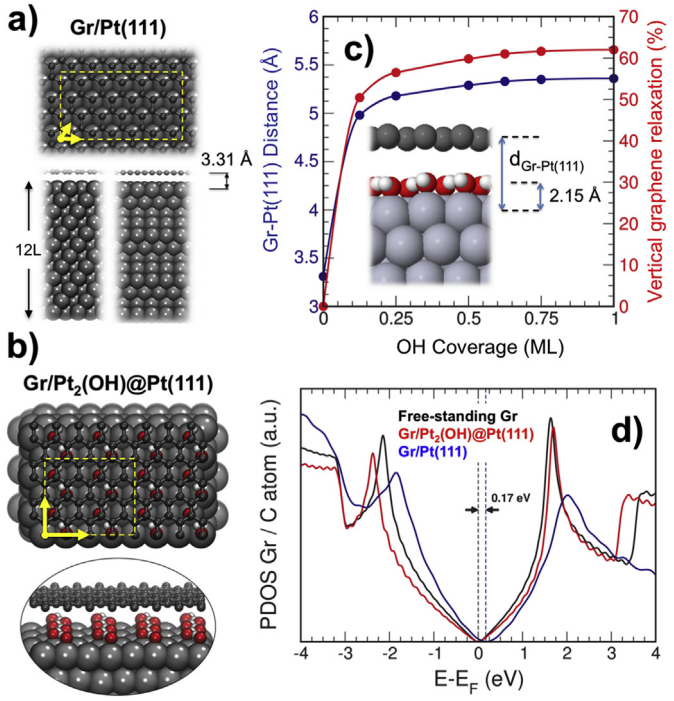

Fig. 6. Top and side view pictorial schemes of: (a) the optimal geometry obtained for the clean Gr/Pt(111) interface with no intercalated-OH content: 0 ML, and (b) the optimized representative Gr/Pt2(OH)@Pt(111) interface with a coverage of 1/2 ML of intercalated-OH between the graphene and the Pt(111) surface. In (a) and (b) H, C, O and Pt atoms correspond to white, grey, red and silver spheres. Yellow arrows indicate the unit cells and dashed-line boxes correspond to the unit cell used in the calculations. (c) Gr—Pt(111) surface perpendicular distance (in Å; blue line) and vertical graphene relaxation degree (in %; red line, see supplementary information for definition) as a function of the coverage (in ML units) of the intercalated-OH. (d) PDOS on the graphene layer for the cases of Gr/Pt(111) (blue line) and Pt2OH (red line) as a function of the energy referred to the Fermi energy (in eV). The canonical DOS of a free-standing SLG is also shown (black line) for a better comparison. (A colour version of this figure can be viewed online.)

seen, from 4.98 to 5.25 Å for an increase in surface OH-content from 0.125 ML to 1 ML, respectively, which tends to saturate for the highest intercalated-OH coverages considered. The physical separation between the graphene and the surface from the 0 ML to the 1 ML case can be quantified as a global expansion of around a 62% in the distance with respect to the Gr/Pt(111) interface (vertical graphene relaxation degree also shown in Fig. 6c calculated as explained in the supplementary information). For a more effective comparison with the experiment, it can be noticed that a remarkable physical decoupling is evident even for the lowest OH coverage theoretically considered (0.125 ML). This agrees with the experimentally demonstrated low intercalated OH coverages where the graphene decoupling process starts to manifest. It is important to remark that from electrochemical charge transfer arguments, a coverage of 0.25 ML of hydroxide was determined. Larger coverage levels can indeed be intercalated, but this amount of hydroxide is enough to structurally lift the graphene layer almost to the saturation value (see Fig. 6c) and induce almost a 90% decoupled surface (Fig. 4 and supplementary information). Larger hydroxyl coverages are thus unnecessary, and we have verified that although these can be induced by using stronger voltammetric treatments, the result is a considerable increase in the number of defects, as was verified by XPS, Raman and AFM.

The main question arising at this point is whether the physical decoupling observed from the calculations will be manifested in an enhanced electronic decoupling of the graphene from the Pt(111) substrate. This can be effectively evaluated by calculating the Projected Density of States (PDOS) on graphene for several representative cases. Fig. 6d shows the PDOS on the graphene layer for the cases of free-standing SLG (black line), 0 ML (Gr/Pt(111): blue line) and 0.5 ML (Gr/Pt_2OH: red line) as a function of the energy referred to the Fermi energy (in eV). Firstly, the PDOS profile for the case of 0 ML reproduces a very well-formed Dirac cone. Nevertheless, the profile morphology is still slightly changed from that obtained for free-standing graphene (black line). Importantly, the PDOS profile for the 0 ML case is not perfectly symmetrical with respect to the Fermi energy, exhibiting a slight p-doping level developed in the graphene layer, in excellent agreement with refs. [55,58,75,77] and references therein. From the calculations, the shift of the Fermi energy between the free-standing graphene and the p-doped graphene case (0 ML) for the Gr/Pt(111) interface of the order of 0.17 eV is similar to those reported by Sutter et al. (0.3 ± 0.15 eV)m [55], Khomyakov et al. (0.3 eV) [75], Yao et al. (0.06 eV) [58], Gao et al. (0.5 eV) [77] and Ferrighi et al. (0.5 eV) [76].

Nevertheless, by inspecting the PDOS profile corresponding to the case of 0.5 ML, it is clearly appreciated that in this case the Dirac-cone is formed by a perfectly symmetrical distribution of the density of states around the Fermi level, which indicates that the slight p-doping existing in graphene for the case of 0 ML has completely disappeared (theory predicts graphene p-doping vanishing even from the 0.125 ML case). This effect may be interpreted as the graphene, with an increasing OH underlayer, decouples electronically, showing a very good agreement with the PDOS profile corresponding to a canonical free-standing graphene layer (black line), in excellent agreement to that recently reported by Ferrighi et al. [76].

4. Summary and perspectives

Summarizing all the experimental and theoretical information presented, we present an effective method to decouple epitaxial graphene from a metal substrate without removing the graphene layer, induced by an electrochemical protocol, and fully describe the decoupling mechanism. UHV graphene growth on transition metals results in a highly pristine single-layer graphene sheet coupled to the surface. This coupling is responsible for the slightly p-type doping of the graphene sheet and the absence of the characteristic G and 2D bands in the Raman spectrum. On removal of the sample from UHV environment the morphology does not change, as shown by AFM. Subsequently the sample is immersed into the electrolyte in an electrochemical cell, and water molecules spontaneously pass through the graphene layer via different structural defects and adsorb on the platinum surface. This spontaneous intercalation occurs in a similar manner to thermally induced intercalation experiments reported by other groups with small molecules. Finally, the application of the appropriate potential activates the reaction between H_2O molecules and the metal surface, forming a single and stable Pt_2OH overlayer, as revealed by charge analysis in the voltammograms and the XPS spectra. As a consequence, the interaction between the graphene sheet and the modified substrate is drastically diminished with respect to the initial state of Gr on Pt(111), leading to the physical separation of the Gr sheet from the surface, as demonstrated by AFM spectroscopic curves and corroborated by DFT calculations, and the emergence of the characteristic graphene peaks G, D and 2D in the Raman spectra. *Ab initio* calculations predict a variation in the distance from the Pt(111) surface of about 1.53 Å after inclusion of the OH layer, and a null charge doping of the graphene sheets and PDOS profiles show a similar behaviour to that of free-standing graphene.

Potential controlled electrochemical oxidation can be applied to

the oxidation/hydroxidation of the surface of many different metals. To date, the understanding of the nature of the reactions that occur under graphene and their optimisation as a graphene decoupling methodology are limited to Pt and Ir (this work and ref 54). However, by carefully controlling the values of electrochemical potential we believe that it should be possible to intercalate a discreet hydroxide (or oxide) layer between the graphene (or other organic) layer and most single crystal metals. Even polycrystalline metals could benefit from this decoupling approach. Clearly this is of great interest for those metals of broader technological impact, such as Cu, Ni, etc., although several difficulties may be encountered related to the innate presence of oxides on the surface.

5. Conclusions

The electrochemical oxidation of epitaxial graphene on Pt(111) and Ir(111) surfaces generates a sandwiched single-hydroxide layer that both structurally and electronically decouples graphene from the metallic substrate without the need for a transfer process. Further optimization of such relatively gentle methodologies applied under ambient conditions could be of considerable interest for avoiding transfer protocols in CVD graphene, opening a pathway to new concepts in the design and construction of graphene-based devices, whilst preserving to some extent the structural integrity of vacuum grown CVD graphene.

Author contributions

I.P. and G. O-I. have grown the UHV samples on Pt and Ir, C.A. performed the electrochemical treatments, E.L. and J.M. the AFM measurements, I.P. the XPS measurements, J.I.M. the DFT calculations, I. M-O., G.J.E. and H.J.S. the Raman spectroscopy. M.F.L. the SEM measurements. J.A.M-G. and G.J.E. conceived the general idea. J.A.M-G. and I.P. were in charge of the overall coordination of the work. The manuscript was written and discussed through contributions of all authors. All authors have given approval to the final version of the manuscript.

Acknowledgements

We acknowledge funding from the Spanish MINECO (Grants MAT2014-54231-C4-1-P, MAT2014-54231-C4-4-P, MAT2013-47898-C2-2-R and MAT2017-85089-C2-1-R), the EU via the ERC-Synergy Program (Grant ERC-2013-SYG-610256 NANOCOSMOS), the innovation program under grant agreement No. 696656 (GrapheneCore1-Graphene-based disruptive technologies), the Comunidad Autónoma de Madrid (CAM) MAD2D-CM Program (S2013/MIT-3007) and computing resources from CTI-CSIC. GOI acknowledges financial support from FCT, Ministry of Science and Technology, Portugal (Grant No. PTDC/CTM-NAN/121108/2010 and IF/01054/2015). EL acknowledges funding from Spanish “Consolider” project CSD2010-00024. JIM acknowledges the financial support by the “Ramón y Cajal” Program of MINECO (Grant RYC-2015-17730) and NANOCOSMOS. We are grateful to Prof. C. Palacio and K. Lauwaet for their help with the XPS measurements.

Appendix A. Supplementary data

Supplementary data related to this article can be found at https://doi.org/10.1016/j.carbon.2017.12.104.

References

[1] K.S. Novoselov, V.I. Fal'ko, L. Colombo, P.R. Gellert, M.G. Schwab, K. Kim, A roadmap for graphene, Nature 490 (2012) 192–200.
[2] A.C. Ferrari, F. Bonaccorso, V. Fal'ko, K.S. Novoselov, S. Roche, Bøggild, et al., Science and technology roadmap for graphene, related two-dimensional crystals, and hybrid systems, Nanoscale 7 (2015) 4598–4810.
[3] Y.M. Lin, C. Dimitrakopoulos, K.A. Jenkins, D.B. Farmer, H.Y. Chiu, A. Grill, et al., 100-GHz transistors from wafer-scale epitaxial graphene, Science 327 (2010) 662.
[4] J.Y. Choi, Graphene transfer: a stamp for all substrates, Nat. Nanotechnol. 8 (2013) 311–312.
[5] J. Kang, D. Shin, S. Bae, B.H. Hong, Graphene transfer: key for applications, Nanoscale 4 (2012) 5527–5537.
[6] R. Muñoz, C. Munuera, J.I. Martínez, J. Azpeitia, C. Gómez-Aleixandre, M. García-Hernández, Low temperature metal free growth of graphene on insulating substrates by plasma assisted chemical vapour deposition, 2D Mater. 4 (2017), 015009.
[7] Z. Yan, Z. Peng, Z. Sun, J. Yao, Y. Zhu, Z. Liu, et al., Growth of bilayer graphene on insulating substrates, ACS Nano 5 (2011) 8187–8192.
[8] R. Wu, L. Gan, X. Ou, Q. Zhang, Z. Luo, Detaching graphene from copper substrate by oxidation-assisted water intercalation, Carbon 98 (2016) 138–143.
[9] J. Kraus, S. Böcklein, R. Reichelt, S. Günther, B. Santos, T.O. Mentes, et al., Towards the perfect graphene membrane? - Improvement and limits during formation of high quality graphene grown on Cu-foils, Carbon 64 (2013) 377–390.
[10] L. Koefoed, M. Kongsfelt, S. Ulstrup, A. Grubišić Čabo, A. Cassidy, P.R. Whelan, et al., Facile electrochemical transfer of large-area single crystal epitaxial graphene from Ir(111), J. Phys. Appl. Phys. 48 (2015), 115306.
[11] V. Miseikis, F. Bianco, J. David, M. Gemmi, V. Pellegrini, M. Romagnoli, et al., Deterministic patterned growth of high-mobility large-crystal graphene: a path towards wafer scale integration, 2D Mater. 4 (2017), 021004.
[12] Z. Salmi, L. Koefoed, B.B.E. Jensen, A. Grubišić Čabo, P. Hofmann, S.U. Pedersen, et al., Electroinduced intercalation of tetraalkylammonium ions at the Interface of graphene grown on copper, platinum, and iridium, ChemElectroChem. 3 (2016) 2202–2211.
[13] L. Gao, W. Ren, H. Xu, L. Jin, Z. Wang, T. Ma, et al., Repeated growth and bubbling transfer of graphene with millimetre-size single-crystal grains using platinum, Nat. Comm 3 (2012) 699.
[14] I.Š. Rakić, D. Čapeta, M. Plodinec, M. Kralj, Large-scale transfer and characterization of macroscopic periodically nano-rippled graphene, Carbon 96 (2016) 243–249.
[15] E. Koren, E. Sutter, S. Bliznakov, F. Ivars-Barcelo, P. Sutter, Isolation of high quality graphene from Ru by solution phase intercalation, Appl. Phys. Lett. 103 (2013) 121602.
[16] S. Schumacher, T.O. Wehling, P. Lazić, S. Runte, D.F. Förster, C. Busse, et al., The backside of graphene: manipulating adsorption by intercalation, Nano Lett. 13 (2013) 5013.
[17] P. Sutter, J.T. Sadowski, E.A. Sutter, Chemistry under cover: tuning metal-graphene interaction by reactive intercalation, JACS 132 (2010) 8175.
[18] C. Romero-Muñiz, A. Martín-Recio, P. Pou, J.M. Gómez-Rodríguez, R. Pérez, Strong dependence of flattening and decoupling of graphene on metals on the local distribution of intercalated oxygen atoms, Carbon 101 (2016) 129.
[19] S. Lizzit, R. Larciprete, P. Lacovig, M. Dalmiglio, F. Orlando, A. Baraldi, et al., Transfer-free electrical insulation of epitaxial graphene from its metal substrate, Nano Lett. 12 (2012) 4503–4507.
[20] S. Gottardi, K. Müller, L. Bignardi, J.C. Moreno-López, T.A. Pham, O. Ivashenko, et al., Comparing graphene growth on Cu(111) versus oxidized Cu(111), Nano Lett. 15 (2015) 917–922.
[21] L. Omiciuolo, E.R. Hernández, E. Miniussi, F. Orlando, P. Lacovig, S. Lizzit, et al., Bottom-up approach for the low-cost synthesis of graphene-alumina nanosheet interfaces using bimetallic alloys, Nat. Comm 5 (2014) 5062.
[22] E. Grånäs, J. Knudsen, U.A. Schröder, T. Gerber, C. Busse, M.A. Arman, et al., Oxygen intercalation under graphene on Ir(111): energetics, kinetics, and the role of graphene edges, ACS Nano 6 (2012) 9951–9963.
[23] A. Preobrajenski, M. Ng, A. Vinogradov, N. Mårtensson, Controlling graphene corrugation on lattice-mismatched substrates, Phys. Rev. B 78 (2008), 073401.
[24] G. Otero, C. González, A.L. Pinardi, P. Merino, S. Gardonio, S. Lizzit, M. Blanco-Rey, et al., Ordered vacancy network induced by the growth of epitaxial graphene on Pt(111), Phys. Rev. Lett. 105 (2010) 216102.
[25] F. Mittendorfer, A. Garhofer, J. Redinger, J. Klimeš, J. Harl, G. Kresse, Graphene on Ni(111): strong interaction and weak adsorption, Phys. Rev. B 84 (2011), 201401(R).
[26] P. Merino, M. Svec, A.L. Pinardi, G. Otero, J.A. Martín-Gago, Strain-driven moiré superstructures of epitaxial graphene on transition metal surfaces, ACS Nano 5 (2011) 5627–5634.
[27] I. Horcas, R. Fernández, J.M. Gómez-Rodríguez, J. Colchero, J. Gómez-Herrero, A.M. Baro, Rev. Sci. Instrum. 78 (2007), 013705.
[28] Alonso C, García-Alonso M C and Escudero M L 2008 Patent nº 200801041, Spain.
[29] P. Giannozzi, S. Baroni, N. Bonini, M. Calandra, R. Car, C. Cavazzoni, et al., QUANTUM ESPRESSO: a modular and open-source software project for quantum simulations of materials, J. Phys. Condens. Matter 21 (2009) 395502.
[30] S. Grimme, Semiempirical GGA-type density functional constructed with a long-range dispersion correction, Comp. Chem. 27 (2006) 1787–1799.
[31] V. Barone, M. Casarin, D. Forrer, M. Pavone, M. Sambi, Vittadini, A Role and effective treatment of dispersive forces in materials: polyethylene and graphite crystals as test cases, Comput. Chem. 30 (2009) 934–939.

[32] Y. Zhang, W. Yang, Comment on "Generalized Gradient Approximation Made Simple", Phys. Rev. Lett. 80 (1998) 890.
[33] A.M. Rappe, K.M. Rabe, E. Kaxiras, J.D. Joannopoulos, Optimized pseudopotentials, Phys. Rev. B 41 (1990) 1227.
[34] N. Mounet, N. Marzari, First-principles determination of the structural, vibrational and thermodynamic properties of diamond, graphite, and derivatives, Phys. Rev. B 71 (2005) 205214.
[35] H.J. Monkhorst, J.D. Pack, Special points for Brillouin-zone integrations, Phys. Rev. B 13 (1976) 5188.
[36] A. Michaelides, P. Hu, A density functional theory study of hydroxyl and the intermediate in the water formation reaction on Pt, J. Chem. Phys. 114 (2001) 513.
[37] J. Azpeitia, G. Otero-Irurueta, I. Palacio, J.I. Martinez, N. Ruiz del Árbol, G. Santoro, et al., High-quality PVD graphene growth by fullerene decomposition on Cu Foils, Carbon 119 (2017) 535–543.
[38] A. Fasolino, J.H. Los, M.I. Katsnelson, Intrinsic ripples in graphene, Nat. Mater. 6 (2007) 858–861.
[39] F. Banhart, J. Kotakoski, A.V. Krasheninnikov, Structural defects in graphene, ACS Nano 5 (2011) 26–41.
[40] H. Angerstein-Kozlowska, B.E. Conway, B. Barnett, J. Mozota, The role of ion adsorption in surface oxide formation and reduction at noble metals: general features of the surface process, J. Electroanal. Chem. 100 (1979) 417–446.
[41] A.M. Gómez-Marín, J. Clavilier, J.M. Feliu, Sequential Pt(111) oxide formation in perchloric acid: an electrochemical study of surface species inter-conversion, J. Electroanal. Chem. 688 (2013) 360–370.
[42] A. Björling, E. Herrero, J.M. Feliu, Electrochemical oxidation of Pt(111) vicinal surfaces: effects of surface structure and specific anion adsorption, J. Phys. Chem. C 115 (2011) 15509–15515.
[43] M.T.M. Koper, J.J. Lukkien, Modeling the butterfly: the voltammetry of $(\sqrt{3}\times\sqrt{3})R30^{\circ}$ and p(2×2) overlayers on (111) electrodes, J. Electroanal. Chem. 485 (2000) 161–165.
[44] A. Berná, V. Climent, J.M. Feliu, New understanding of the nature of OH adsorption on Pt(111) electrodes, Electrochem. Commun. 9 (2007) 2789–2794.
[45] X. Feng, S. Maier, M. Salmeron, Water splits epitaxial graphene and intercalates, J. Am. Chem. Soc. 134 (2012) 5662–5668.
[46] Y. Yao, Q. Fu, Y.Y. Zhang, X. Weng, H. Li, M. Chen, et al., Graphene cover-promoted metal-catalyzed reactions, Proc. Natl. Acad. Sci. 111 (2014) 17023–17028.
[47] R. Mu, Q. Fu, L. Jin, L. Yu, G. Fang, D. Tan, et al., Visualizing chemical reactions confined under graphene, Angew. Chem. Int. Ed. 51 (2012) 4856–4859.
[48] R. Hawaldar, P. Merino, M.R. Correia, I. Bdikin, J. Grácio, J. Méndez, et al., Large-area high-throughput synthesis of monolayer graphene sheet by hot filament thermal chemical vapor deposition, Sci. Rep. 2 (2012) 682.
[49] M. Wakisaka, H. Suzuki, S. Mitsui, H. Uchida, M. Watanabe, Identification and quantification of oxygen species adsorbed on Pt(111) single-crystal and polycrystalline Pt electrodes by photoelectron spectroscopy, Langmuir 25 (2009) 1897–1900.
[50] M.A. Henderson, The interaction of water with solid surfaces: fundamental aspects revisited, Surf. Sci. Rep. 46 (2002) 1–308.
[51] C.R. Parkinson, M. Walker, C.F. McConville, Reaction of atomic oxygen with a Pt(111) surface: chemical and structural determination using XPS, CAICISS and LEED, Surf. Sci. 545 (2003) 19–33.
[52] R.L. Schwiesow, V.E. Derr, A Raman scattering method for precise measurement of atmospheric oxygen balance, J. Geophys. Res. 75 (1970) 1629–1632.
[53] N.J. Kang, J.H. Mun, C.Y. Hwang, B.J. Cho, Monolayer graphene growth on sputtered thin film platinum, J. Appl. Phys. 106 (2009) 104309.
[54] Y. Fu, A.V. Rudnev, G.K.H. Wiberg, M. Arenz, Single Graphene Layer on Pt(111) Creates Confined Electrochemical Environment via Selective Ion Transport, Angew. Chem. Int. Ed. 56 (2017) 1–6.
[55] P. Sutter, J.T. Sadowski, E. Sutter, Graphene on Pt(111): growth and substrate interaction, Phys. Rev. B 80 (2009), 245411.
[56] A. Zettl, Q. Zhou, APS March Meeting, 2013.
[57] Q. Zhou, S. Coh, M.L. Cohen, S.G. Louie, A. Zettl, Imprint of transition metal *d* orbitals on a graphene Dirac cone, Phys. Rev. B 88 (2013) 235431.
[58] W. Yao, E. Wang, K. Deng, S. Yang, W. Wu, A.V. Fedorov, et al., Monolayer charge-neutral graphene on platinum with extremely weak electron-phonon coupling, Phys. Rev. B 92 (2015) 115421.
[59] L.M. Malard, M.A. Pimenta, G. Dresselhaus, M.S. Dresselhaus, Raman spectroscopy in graphene, Phys. Rep. 473 (2009) 51–87.
[60] A.C. Ferrari, Raman spectroscopy of graphene and graphite: Disorder, electron–phonon coupling, doping and nonadiabatic effects, Solid State Commun. 143 (2007) 47–57.
[61] M. Malard, D.L. Mafra, S.K. Doorn, M.A. Pimenta, Resonance Raman scattering in graphene: Probing phonons and electrons, Solid State Commun. 149 (2009) 1136–1139.
[62] A.C. Ferrari, J.C. Meyer, V. Scardaci, C. Casiraghi, M. Lazzeri, F. Mauri, et al., Raman Spectrum of Graphene and Graphene Layers, Phys. Rev. Lett. 97 (2006), 187401.
[63] E. Cazzanelli, T. Caruso, M. Castriota, A.R. Marino, A. Politano, G. Chiarello, et al., Spectroscopic characterization of graphene films grown on Pt(111) surface by chemical vapor deposition of ethylene, J. Raman Spectrosc. 44 (2013) 1393–1397.
[64] J.I. Martínez, P. Merino, A.L. Pinardi, G. Otero-Irurueta, M.F. López, J. Méndez, et al., Role of the pinning points in epitaxial graphene moiré superstructures on the Pt(111) Surface, Sci. Rep. 6 (2016) 20354.
[65] J. Avila, I. Razado, S. Lorcy, E. Pichonat, D. Vignaud, X. Wallart, et al., Exploring electronic structure of one-atom thick polycrystalline graphene films: a nano angle resolved photoemission study, Sci. Rep. 3 (2013) 2439.
[66] A. Barinov, O.B. Malcioğlu, S. Fabris, T. Sun, L. Gregoratti, M. Dalmiglio, et al., Initial stages of oxidation on graphitic surfaces: photoemission study and density functional theory calculations, J. Phys. Chem. C 113 (2009) 9009–9013.
[67] G.V. Bianco, M. Losurdo, M.M. Giangregorio, P. Capezzuto, G. Bruno, Exploring and rationalising effective n-doping of large area CVD-graphene by NH_3, Phys. Chem. Chem. Phys. 16 (2014) 3632–3639.
[68] A.L. Pinardi, Tailoring On-surface Chemistry of (Hetero)aromatics on Transition Metal Surfaces, Ph.D. Thesis, CSIC – Institute of Material Science of Madrid (ICMM)/Autonomous University of Madrid, 2013.
[69] R. Larciprete, S. Ulstrup, P. Lacovig, M. Dalmiglio, M. Bianchi, F. Mazzola, et al., Oxygen Switching of the Epitaxial Graphene Metal Interaction, ACS Nano 6 (2012) 9551–9558.
[70] H.J. Butt, B. Cappella, M. Kappl, Force measurements with the atomic force microscope: technique, interpretation and applications, Surf. Sci. Rep. 59 (2005) 1–152.
[71] W. Zhu, T. Low, V. Perebeinos, A.A. Bol, Y. Zhu, H. Yan, et al., Structure and Electronic Transport in Graphene Wrinkles, Nano Lett. 12 (2012) 3431–3436.
[72] W. Wang, S. Yang, A. Wang, Observation of the unexpected morphology of graphene wrinkle on copper substrate, Sci. Rep. 7 (2017) 8244.
[73] H. Wolfschmidt, C. Baier, S. Gsell, M. Fischer, M. Schreck, U. Stimming, STM, SECPM, AFM and Electrochemistry on Single Crystalline Surfaces, Materials 3 (2010) 4196–4213.
[74] R. Gómez, M.J. Weaver, Reduction of Nitrous Oxide on Iridium Single-Crystal Electrodes, Langmuir 18 (2002) 4426–4432.
[75] P.A. Khomyakov, G. Giovannetti, P.C. Rusu, G. Brocks, J. van den Brink, P.J. Kelly, First-principles study of the interaction and charge transfer between graphene and metals, Phys. Rev. B 79 (2009) 195425.
[76] L. Ferrighi, D. Perilli, D. Selli, C. Di Valentin, Water at the interface between defective graphene and Cu or Pt (111) surfaces, Appl. Mater. Interfaces 9 (2017) 29932–29941.
[77] M. Gao, Y. Pan, L. Huang, H. Hu, L.Z. Zhang, H.M. Guo, et al., Epitaxial growth and structural property of graphene on Pt(111), Appl. Phys. Lett. 98 (2011), 033101.